Geometrical Effects on the Temperature Distribution in a Half-Space Due to a Moving Heat Source

Mohsen Akbari[1]
Mechatronic Systems Engineering,
School of Engineering Science,
Simon Fraser University,
Surrey, BC, V3T 0A3, Canada
e-mail: mohsen_akbari@sfu.ca

David Sinton
Department of Mechanical Engineering,
University of Victoria,
Victoria, BC, V8W 2Y2, Canada

Majid Bahrami
Mechatronic Systems Engineering,
School of Engineering Science,
Simon Fraser University,
Surrey, BC, V3T 0A3, Canada

Fundamental problem of heat transfer within a half-space due to a moving heat source of hyperelliptical geometry is studied in this work. The considered hyperelliptical geometry family covers a wide range of heat source shapes, including star-shaped, rhombic, elliptical, rectangular with round corners, rectangular, circular, and square. The effects of the heat source speed, aspect ratio, corners, and orientation are investigated using the general solution of a moving point source on a half-space and superposition. Selecting the square root of the heat source area as the characteristics length scale, it is shown that the maximum temperature within the half-space is a function of the heat source speed (Peclet number) and its aspect ratio. It is observed that the details of the exact heat source shape have negligible effect on the maximum temperature within the half-space. New general compact relationships are introduced that can predict the maximum temperature within the half-space with reasonable accuracy. The validity of the suggested relationships is examined by available experimental and numerical data for the grinding process, for medium Peclet numbers. For ultrafast heat sources, an independent experimental study is performed using a commercial CO_2 laser system. The measured depth of the engraved grooves is successfully predicted by the proposed relationships.
[DOI: 10.1115/1.4003155]

Keywords: moving heat source, half-space, temperature distribution, arbitrary geometry, modeling

1 Introduction

The problem of stationary and moving heat sources applies to many fields of engineering such as metal cutting, spot welding, laser cutting, laser surface treatment, friction between mechanical parts, and tribological applications including ball bearing and gear design [1–5]. In many circumstances, the size of the heat source compared to the conducting body is small enough that a heat source on a half-space assumption can be made. There are many studies in the literature that focused on finding the transient and quasi-steady temperature distribution within a half-space due to a moving heat source; examples are listed in Table 1.

Among the available references, there are few that deal with various geometric shapes of heat sources [6–8]. Tian and Kennedy, Jr. [6] used a combination of point source solution [9] and the Green's function method to develop accurate correlations for the circular and square heat sources. These correlations were used to formulate models for predicting flash temperatures (i.e., maximum surface temperature) in sliding asperities for any speed. Using the classical point solution, Hou and Komanduri [7] developed a general solution for elliptical and rectangular heat sources with different heat flux intensities of uniform, parabolic, and normal. Their method requires different length scales and constant parameters for different geometries to compute the temperature distribution within a half-space. Muzychka and Yovanovich [10] showed that the thermal resistance of a moving heat source is a weak function of source shape if the square root of the heat source area is selected as a characteristic length scale in all calculations. Based on this argument and using the solutions for stationary and ultrafast heat sources, they [10] proposed a general solution to predict the thermal resistance of a moving heat source of arbitrary shape. Most recently, Laraqi et al. [8] used the Fourier transform to investigate the maximum contact temperature for three configurations: (i) rectangular source on a rectangular prism, (ii) elliptic source on a rectangular prism, and (iii) eccentric circular source on a rotating cylinder. By varying the values of geometric parameters in the provided solutions, they [8] proposed a solution for various particular cases such as strip, rectangular, square, elliptic, and circular moving heat sources.

Present work discusses various aspects of the fundamental problem of heat transfer within a half-space due to a moving heat source of arbitrary shape. This paper has two objectives: (i) perform a systematic study on the relevant geometrical parameter effect on the maximum temperature within a half-space due to a moving heat source of arbitrary but symmetrical shape (this will eventually lead to simplified models for an arbitrarily shaped moving heat source) and (ii) present new compact relationships for the hyperelliptical family of heat sources, which provide analytical-based compact solutions that are essential for basic designs, parametric studies, and optimization analyses required for many engineering applications. The hyperelliptical geometry is considered since it covers a wide variety of symmetrical shapes including the star-shaped, rhombic, elliptical, circular, rectangular, and squared. The proposed model is validated with numerical and experimental data from different studies for rectangular and square geometries. Moreover, a CO_2 laser system is used to engrave grooves on wooden substrates over a wide range of laser power and the beam speed. Measured depth are compared against those predicted by the theory presented in this work with acceptable accuracy.

2 Theory

Figure 1 schematically shows the geometry of a symmetrical moving heat source of arbitrary shape on a half-space. The mathematical problem consists in finding the solution for temperature rise defined as $\theta = T(R,t) - T_0$, where T_0 is a reference temperature, for any point in the moving coordinate of $(X = x - Ut, y, z)$ to the three dimensional diffusion equation with constant thermal properties (see Fig. 1) [11],

$$\nabla^2\theta - \frac{U}{\alpha}\frac{\partial\theta}{\partial X} = \frac{1}{\alpha}\frac{\partial\theta}{\partial t}$$

Initial condition:

$$\theta = 0, \quad t = 0 \quad \text{everywhere}$$

[1]Corresponding author.

Contributed by the Heat Transfer Division of ASME for publication in the JOURNAL OF HEAT TRANSFER. Manuscript received February 26, 2010; final manuscript received November 24, 2010; published online March 2, 2011. Assoc. Editor: Oronzio Manca.

Table 1 Summary of previous studies on moving heat source in the literature

Author	Year	Method	Source shape	Heat flux	Comments
Carslaw and Jeager [9]	1959	A	Point, line, and infinite strip	Uniform	- Introduced the heat source approach.
Takazawa [26]	1966	N	Infinite strip	Uniform	- Approximate relationship for the maximum temperature rise within a half-space as a function of Peclet number. - Width of the source in the moving direction as a length scale.
Paek and Gagliano [27]	1972	A/E	Circle	Uniform	- Half-space and finite body. - Instantaneous point source method. - Transient solution in the form of the modified Bessel function of first kind. - Integral over the surface of the heat source is numerically solved.
Weichert and Schonert [12]	1978	A	Line, plane, and cube	Uniform	- Exponential transformation is used. - Effect of aspect ratio and source speed are numerically investigated.
Eager and Tsai [28]	1983	A/E	Circle	Gaussian	- Superposition of instantaneous point sources with different powers. - Single integral that is solved numerically. - Heat source radius as the length scale.
Terauchi et al. [13]	1985	A	Rectangle, square, and circle	Uniform/parabolic	- Single and double heat sources. - Effect of the aspect ratio is investigated. - Width of the source in the moving direction and source radius as the length scale for rectangular and circular heat sources, respectively.
Zhang [29]	1990	A	Thin rod and infinite plane	Uniform	- Transient solutions for 1D problem in an infinite body.
Tian and Kennedy, Jr. [6]	1995	A	Ellipse/rectangle	Uniform/parabolic	- Green's function method and point source method are used. - Maximum and average surface temperatures are obtained for the entire range of Peclet numbers. - Length scale is the diameter/width of the circular/square source.
Manca et al. [30]	1995	A	Circle	Gaussian	- Three dimensional problem in a finite body is solved using Green's function method. - Source radius as the length scale.
Yevtushenko et al. [31]	1997	A	Circle	Uniform	- Transient problem is solved using a finite Fourier transform. - Final solution is in the form of an infinite integral of the Bessel functions of first and second kinds. - Source diameter as the length scale.
Zeng et al. [32]	1997	A	Cylinder (thin rod)	General	- General transient solutions in the form of an infinite series.
Zubair and Chaudhry [33,34]	1996/1998	A	Point source and infinite plane	Uniform but time dependent	- Transient problem is solved.
Kato and Fujii [35]	1997	E	Infinite strip	Uniform	- Temperature measurement using PVD films. - Maximum temperature rise for different grinding wheel materials is reported at different locations within the workpiece. - Source width as the length scale.
Kaebernick et al. [36]	1999	A/E	Circle	Gaussian	- Pulsed laser is considered. - Proposed models are in the form of double integrals.
Neder et al.[37]	1999	N	Circle	Uniform	- Finite element method is used. - Source diameter as the length scale and entire range of Peclet numbers are investigated.

Table 1 (***Continued.***)

Author	Year	Method	Source shape	Heat flux	Comments
Hou and Komanduri [7]	2000	A	Ellipse/rectangle	Parabolic, uniform, and normal	- General solution based on the point source method is proposed. - Final solution in the form of triple integrals. - Different length scales are used for different source shapes. - Approximate relationship is proposed elliptical heat source and uniform and normal flux.
Xu and Malkin [25]	2001	E	Infinite strip	Uniform	- Comparison between three different grinding temperature measurement techniques.
Muzychka and Yovanovich [10]	2001	A	Arbitrary shape	Uniform, parabolic, isothermal	- Thermal resistance for arbitrary shape contacts is investigated. - Approximate relationship is proposed for uniform and parabolic distribution square root of source area as the length scale.
Vick and Furey [24]	2003	A	Square	Uniform	- Single and multiple heat sources are considered. - Surface temperature distribution is reported for 20 different materials. - Width of the source as a length scale.
Baïri [38]	2003	A	Circle	Uniform	- Thermal resistance due to moving multiple sources. - Two layer half-space is studied. - Models are in the form of double series. - Source diameter as the length scale.
Laraqi et al. [8]	2004	A	Ellipse/rectangle	Uniform	- Three configurations are investigated: (i) rectangular source on a rectangular prism, (ii) elliptic source on a rectangular prism, and (iii) eccentric circular source on a rotating cylinder. - Fourier transform is used. - Square root of the source area as a length scale for the dimensionless temperature and source major axis/width along the moving direction for Peclet number.
Li et al. [39]	2004	A/N/E	Circle	Gaussian	- Volumetric and surface heating are compared for quasi-steady solution. - Green's function method is used. - Source diameter as the length scale.
Kuo and Lin [40]	2006	A	Rectangle	Uniform	- Temperature distribution due to the grinding process is investigated.
Bianco et al. [41]	2006	N	Circle	Gaussian	- Transient temperature distribution is solved using the FE method.
Wen and Khonsari [42]	2007	A	Infinite strip	Uniform/ oscillatory	- 2D temperature distribution due to an oscillatory heat flux is obtained using Duhamel's theorem and finite element method.
Levin [43]	2008	A	Line/circle	Uniform, Gaussian	- General solution using the method of images is obtained for quasi-steady solution. - Trailing temperature is well captured by this method. - Final solution in the form of the green function and double integrals.
Laraqi et al. [44]	2009	A	Circle	Uniform	- Governing equations are solved for both a circular pin and a rotating disk. - Fourier and finite Henkel integral transforms are used. - Source diameter as the length scale.
Xu et al. [45]	2010	A/N/E	Square	Uniform	- Laser quenching of cylindrical workpiece is investigated based on the point source method is proposed. - FE numerical validation is performed followed by experiments using a CO_2 laser system.

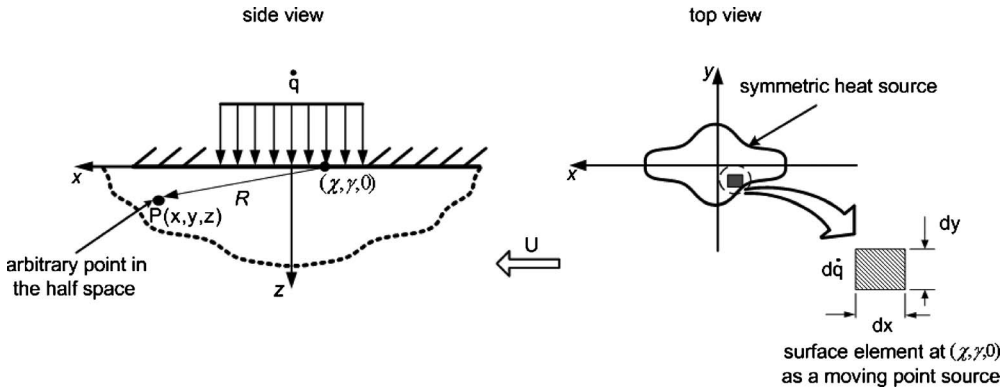

Fig. 1 Schematic of a symmetrical moving plane heat source with arbitrary shape

Boundary conditions:

$$-k\left(\frac{\partial\theta}{\partial z}\right)_{z=0}=\dot{q} \quad \text{(on the heat source)}$$

$$-k\left(\frac{\partial\theta}{\partial z}\right)_{z=0}=0 \quad \text{(elsewhere)}$$

$$T_{x,y,z\to\infty}=0 \tag{1}$$

The solution to Eq. (1) for a hyperelliptical heat source defined as $(X^*/\alpha^*)^n+(y^*/b^*)^n=1$, can be obtained by superposition of point sources [7,12] over the heat source area in the dimensionless moving coordinate of $(X^*=X/\mathcal{L}, y^*=y/\mathcal{L}, z^*=z/\mathcal{L})$

$$\theta^*=\int_{-a^*}^{a^*}\int_{-\varepsilon_m a^*[1-(\chi/a^*)^n]^{1/n}}^{\varepsilon_m a^*[1-(\chi/a^*)^n]^{1/n}}\frac{e^{-\mathrm{Pe}(X^*-\chi^*)}}{4\pi R^*}\left\{e^{\mathrm{Pe}R^*}\,\mathrm{erfc}\left(\frac{R^*}{2\sqrt{\mathrm{Fo}}}+\mathrm{Pe}\sqrt{\mathrm{Fo}}\right)+e^{-\mathrm{Pe}R^*}\,\mathrm{erfc}\left(\frac{R^*}{2\sqrt{\mathrm{Fo}}}-\mathrm{Pe}\sqrt{\mathrm{Fo}}\right)\right\}d\gamma^*d\chi^* \tag{2}$$

where a^* and b^* are the dimensionless major and minor axes, n determines the shape of the geometry (see Fig. 2), $\theta^*=\theta k/\dot{q}\mathcal{L}$, $\mathrm{Pe}=U\mathcal{L}/2\alpha$, $\mathrm{Fo}=\alpha t/\mathcal{L}^2$, $\mathcal{L}$ is the characteristic length, and $R^*=\sqrt{(X^*-\chi^*)^2+(y^*-\gamma^*)^2+z^{*2}}$. The hyperellipse yields many special cases by setting the values of n and the aspect ratio $\varepsilon_m=b/a$. Therefore, the solution developed for the hyperellipse can be used to analyze a variety of geometries, including star shapes, ellipses, circles, rectangles, squares, diamondlike geometries, and line sources. Note that ε_m accounts for the effect of the heat source orientation and can have any value in the range of $0<\varepsilon_m<\infty$.

Selection of the characteristic length, $\mathcal{L}$, is an arbitrary choice and can be defined for each geometry individually. For instance, for a circular or square source, the best choices are the source diameter and width, respectively [6]. For an elliptical or rectangular source, on the other hand, the axis of the source in the moving direction can be selected as the length scale [7,13]. When dealing with an arbitrary geometry, it is essential to select an appropriate length scale to obtain more consistent results. It is demonstrated [14,15] that for stationary heat sources when the square root of the heat source area, $\sqrt{A}$, is chosen as the characteristic length scale, similar trends for various heat source shapes are obtained. We examined this length scale (i.e., $\sqrt{A}$) for moving heat sources later by using $\mathcal{L}=\sqrt{A}$, consistently throughout the present analysis.

A closed form solution for Eq. (2) cannot be found even for simple geometries such as ellipse or rectangle; thus, we solved it numerically. An in-house computational code is developed in MAPLE 11 [16] to solve the double integral in Eq. (2). To ensure that the same heat flow rate enters the half-space for different geometries, the total source area is kept constant throughout the

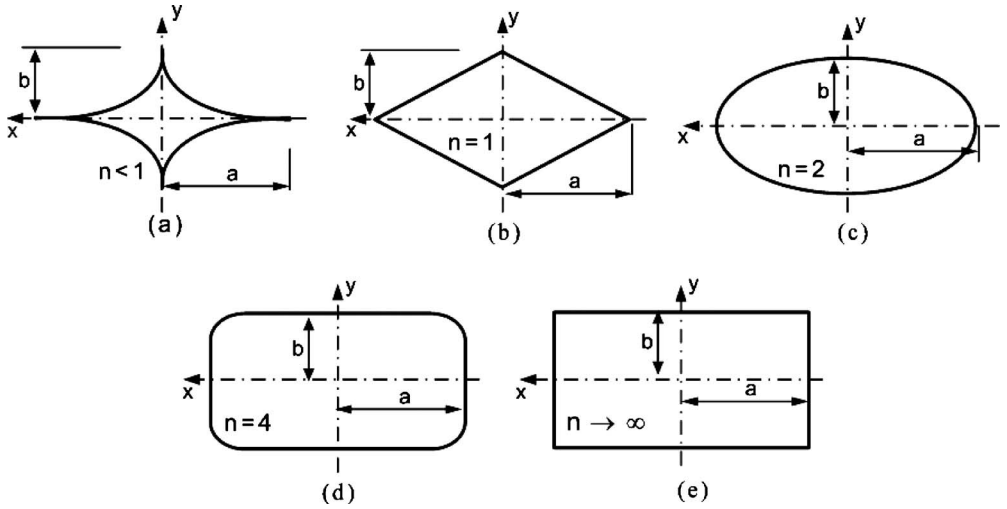

Fig. 2 Hyperellipse as a general symmetric geometry covers an array of source geometries: (*a*) star shape (n<1), (*b*) rhombic (n=1), (*c*) elliptical (n=2), (*d*) rectangular with round corners (n=4), and (*e*) rectangular (n→∞)

entire analysis. It should be noted that in Eq. (2), quasi-steady condition is achieved very fast (e.g., for a typical value of Pe $=10$, the transition times for the steady-state condition for a 1×1 mm^2 square heat source are 20 ms and 400 ms for stainless steel and wood, respectively). Hence, in most applications, it can be assumed that the quasi-steady condition is reached very fast; thus, only steady-state condition is considered though this work.

3 Experimental Study

3.1 Test Procedure. Grooves were ablated in wooden (red oak) surfaces using a CO_2 laser system (Universal Laser system, model VSL 3.60, Scottsdale). The system has a CO_2 laser cartridge rated at a maximum power of $60 \pm 10\%$ W that produces an invisible continuous infrared beam at a wavelength of 10.6 μm. The movement of the mirrors and lens assembly is achieved by a motor and controlled by an operating software. The laser system works with vector and raster modes to produce lines and filled shapes, respectively. The system was set to vector mode for single pass ablation in this work. Laser power and speed were set as a percentage of maximum using the laser control software. The system was rated to run at the maximum raster beam speed of 255 mm/s $\pm 2\%$ (45 in./s) according to the manufacturer. Since the maximum vector mode speed was lower than the raster mode, the beam speed in the vector mode was determined by measuring the amount of time required for the beam to engrave a straight line with a specific length. The focal length of the lens was 50.8 mm $\pm 4\%$ (2 in.), which according to the manufacturer specifications generated a circular spot size of 127 μm $\pm 4\%$ (0.005 in.). The laser was focused by controlling the "z" position of the workstation for different material thicknesses. The measurement showed that the percentage system changed the beam speed proportionally with respect to the maximum speed, which corresponds to the Peclet number of Pe $=130 \pm 12\%$.

Commercial red oak was purchased with the thickness of 7 mm $\pm 8\%$ and was cut to form rectangular 30×60 mm^2 substrates. Red oak was used because of its opacity, with an absorption coefficient of $0.91 \pm 5\%$ [17] at the wavelength of 10.6 μm. Moreover, red oak does not melt during the pre-ignition process, and its radiative ignition temperature is available in the literature [17–20]. The opacity of the material helps to assume that the external radiation is absorbed at the surface of the substrate. The substrate width and height were large enough to ensure the half-space assumption. Following the laser exposure, the channel depth was determined by taking the images of channel cross-section using a charge coupled device (CCD) camera mounted on an inverted microscope (Unitron, Commack, NY) at the magnification of 10×. Figure 3 shows the schematic diagram of the laser beam, the engraved groove, and the cross-sectional image of the wooden substrate (red oak) following laser exposure at the typical relative beam speed of $U^*=U/U_{\max}=0.6$ and relative power of $P^*=P/P_{\max.}=0.4$. Images were analyzed in the image processing software (ScopePhoto 2.0) in which each pixel is calibrated using a 20 line/mm optical ruler (Edmund Optics, Barrington, NJ). Laser ablation of red oak is a complicated process that includes production of char and endothermic decomposition [19,21]. However, these effects are not considered in this work, and the surface of each channel is assumed to be an isotherm with the red oak burning temperature of θ_b. This simplification is shown to be valid for a wide range of beam speed and laser power.

3.2 Uncertainty Analysis. The groove depth, d_g, is a complex function of laser power, $\dot{q}$, beam speed, U, spot size, d_s, thermal diffusivity, α, and absorption coefficient, ω. The maximum uncertainty for the groove depth measurements can be calculated from [22]

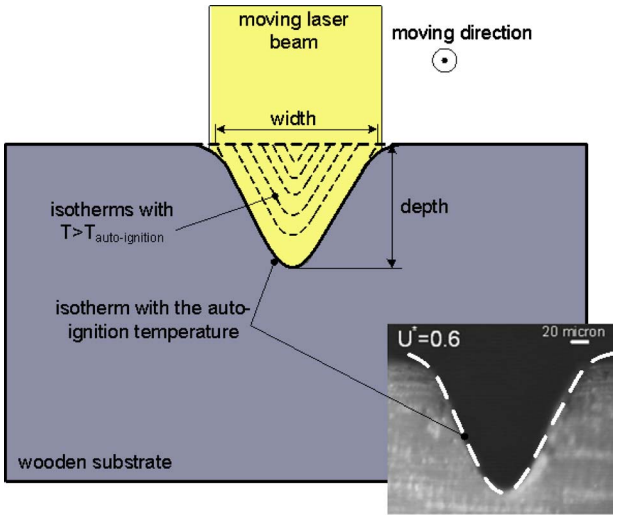

Fig. 3 Schematic diagram of the laser beam, the engraved groove, and cross-sectional image of the wooden substrate (red oak) following laser exposure at the typical relative beam speed of $U^*=U/U_{max}=0.6$ and relative power of $P^*=P/P_{max.}=0.4$. Image is taken by an inverted microscope (Unitron, Commack, NY) with a 10× magnification.

$$\frac{\delta d_g}{d_g} = \sqrt{\left(\frac{\delta \dot{q}}{\dot{q}}\right)^2 + \left(\frac{\delta U}{U}\right)^2 + \left(\frac{\delta d_s}{d_s}\right)^2 + \left(\frac{\delta \alpha}{\alpha}\right)^2 + \left(\frac{\delta \omega}{\omega}\right)^2} \quad (3)$$

With the maximum estimated uncertainties of the relevant parameters listed in Table 2, the maximum uncertainty is estimated to be $\pm 13.9\%$.

4 Parametric Study and Approximate Models

The influence of the relevant important parameters on the temperature distribution due to a moving plane source is investigated. The effects of the shape parameter, n, the heat source aspect ratio, ε_m, and the source speed (Peclet number, Pe), on the temperature field within the half-space at quasi-steady condition are discussed in detail in the following subsections. The trends of the results are studied for a range of each parameter, while the remaining parameters are held constant. The heat source area is kept constant through the entire study to ensure that the same heat flow enters the half-space.

4.1 Shape Parameter, n. The variation in the maximum temperature, $\theta^*_{\max}$, within the half-space with respect to the shape parameter, n, is plotted in Fig. 4 for two typical values of aspect ratios: $\varepsilon_m=0.1$ and 0.5 and Peclet number of Pe $=10$. The solid lines represent the mean values of calculated results. As can be seen, the effect of the heat source corners on the maximum temperature is small (within $\pm 2\%$ of the average value) and thus can be neglected.

4.2 Aspect Ratio, ε_m. Figure 5 shows the variation in the maximum temperature, $\theta^*_{\max}$, with aspect ratio on the surface of a rectangular heat source for different values of Peclet number. For

Table 2 Estimated uncertainty of involving parameters in the analysis

$\delta\dot{q}/\dot{q}$	$\delta U/U$	$\delta d_s/d_s$	$\delta\alpha/\alpha$	$\delta\omega/\omega$
11.1%	2%	3.9%	5%	5%

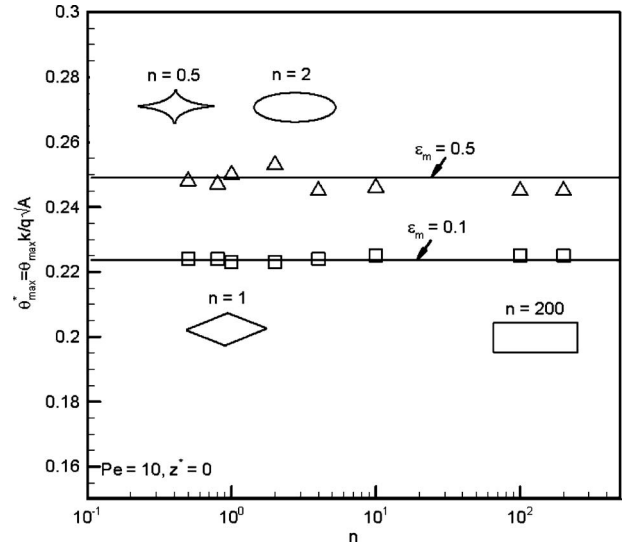

Fig. 4 Effect of heat source shape on the quasi-steady maximum temperature for two typical aspect ratios, 0.1 and 0.5, and Peclet number of Pe=10

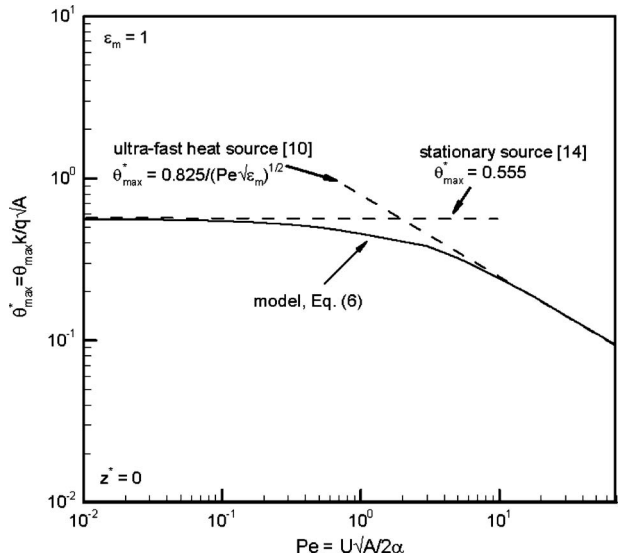

Fig. 6 Maximum temperature as a function of Peclet number for aspect ratio of ε_m=1, a typical value. Note that two asymptotes for stationary, Pe→0, and fast moving heat source, Pe →∞, can be recognized in the present plot.

very slow heat sources, (i.e., Pe→0), the maximum temperature within a half-space can be obtained from the stationary heat source solution [14],

$$\theta^*_{\max,s} = \sqrt{\frac{\varepsilon_s}{\pi}}\left[\frac{\sinh^{-1}(\varepsilon_s)}{\varepsilon_s} + \sinh^{-1}\left(\frac{1}{\varepsilon_s}\right)\right] \tag{4}$$

where $\theta^*_{\max,s}$ is the maximum temperature due to a stationary heat source. The aspect ratio of a stationary heat source is denoted by $\varepsilon_s = b/a$ such that $0 < \varepsilon_s \leq 1$. Equation (4) shows that for a stationary heat source, the highest maximum temperature occurs at the aspect ratio of 1 (e.g., square or circle). For a moving heat source, as the source speed increases, (i.e., Peclet number increases), the maximum temperature drops, the peak in the plot occurs to the lower aspect ratios, and the effect of the source orientation becomes less significant (see Fig. 5). This means that for heat sources with similar speed and areas, those which are elongated in the direction of motion have higher temperatures. For very high Peclet numbers, i.e., Pe~$0(10^2)$, it can be shown that $\theta^*_{\max} \propto \mathrm{Pe}^{-1.2}\varepsilon_m^{-1/4}$ [10].

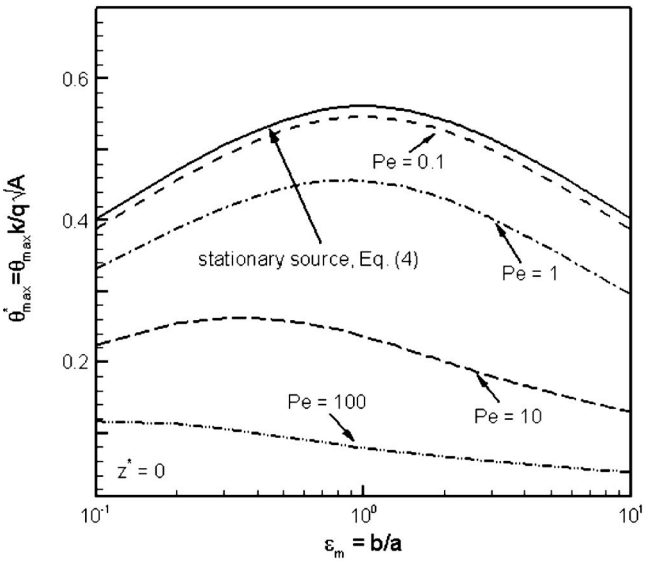

Fig. 5 Effect of the aspect ratio on the maximum temperature of a plane moving heat source at various source speeds (Peclet number)

4.3 Source Speed, Pe. Variation in the maximum surface temperature as a function of Peclet number for a typical aspect ratio of ε_m=1 is plotted in Fig. 6. When a heat source moves at higher speeds, it spends shorter time at each spot; thus, less heat is transferred to the half-space and the maximum temperature decreases. Two asymptotes can be recognized for each aspect ratio: (a) very slow (Pe→0) and (b) ultrafast moving heat source (Pe →∞). The maximum surface temperature for low Peclet numbers (i.e., Pe<0.1) can be obtained from Eq. (4). Since the source corners have negligible effect on the maximum temperature [14,15], Eq. (4) can be applied to other geometries such as ellipse, rhombic, star-shape, and rectangle with rounded corners with reasonable accuracy. For ultrafast moving heat sources (i.e., Pe→∞), Muzychka and Yovanovich [10] used the same approach of Jaeger [23] to obtain the maximum temperature due to an elliptical heat source as a function of Peclet number and aspect ratio. Comparing to the relationship provided by Jaeger [23] for a rectangular shape, it can be observed that the maximum temperature of an elliptical heat source ($n \to 2$) is 6.25% higher than that of a rectangular heat source ($n \to \infty$) with the same area. Following the approach of Muzychka and Yovanovich [10], Eq. (5) is developed for ultrafast finite moving heat sources of hyperelliptical shapes,

$$\theta^*_{\max,f} = \frac{0.825}{(\mathrm{Pe}\sqrt{\varepsilon_m})^{1/2}} \tag{5}$$

where $\theta^*_{\max,f}$ is the maximum temperature rise due to a fast moving heat source. Equation (5) accurately predicts the maximum surface temperature over the range of $0.5 \leq \varepsilon_m \leq 1$.

4.4 Distance From the Source Surface, z^*. In Fig. 7, the maximum temperature at different z-planes, $\theta^*_{\max}(z^*)$, is nondimensionalized with respect to the maximum temperature at the surface of the half-space, $\theta^*_{\max,0}$, and plotted against the dimensionless depth for three typical aspect ratios of 0.1, 0.5, and 1. Two geometries are considered: rectangle with a typical Peclet number of Pe=10 and stationary elliptical source. It can be seen that the temperature decreases rapidly at points near the heat

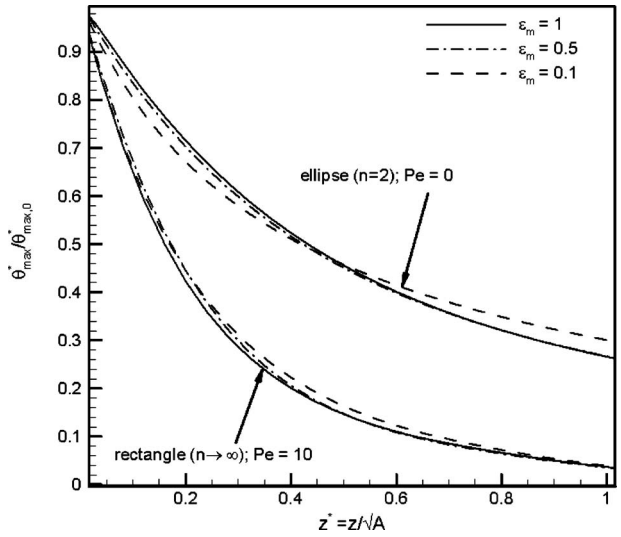

Fig. 7 Variation in $\theta^*_{max}/\theta^*_{max,0}$ as a function of dimensionless depth for elliptical (n→2) and rectangular (n→∞) heat sources with Pe=10 and various aspect ratios

source surface followed by a gradual change with increasing depth. Interestingly, although $\theta^*_{max}/\theta^*_{max,0}$ changes with the Peclet number, it is independent of both the corners (n) and the aspect ratio (ε_m).

4.5 Approximate Model. To develop a general compact relationship for the maximum temperature, we use the asymptotic blending method of Churchill and Usagi [36]. This method allows the combination of asymptotic solutions to generate a model that is valid for all values of the dependent parameter as follows:

$$\theta^*_{max,0} = \left[\frac{1}{(\theta^*_{max,s})^m} + \frac{1}{(\theta^*_{max,f})^m}\right]^{-1/m} \tag{6}$$

where $\theta^*_{max,s}$ and $\theta^*_{max,f}$ are obtained from Eqs. (4) and (5), respectively, and m is a correlation parameter. A single value of $m=2$ was found to give excellent agreement between the model and the solution of Eq. (2). Note that variation in $\theta^*_{max,s}$ with respect to the heat source aspect ratio is negligible for $0.5 \le \varepsilon_s \le 1$, and the average value of $\theta^*_{max,s}=0.555$ can be used instead of Eq. (4). Therefore, Eq. (6) reduces to

$$\theta^*_{max,0} = [3.240 + 1.474\mathrm{Pe}\sqrt{\varepsilon_m}]^{-1/2}, \quad 0.5 \le \varepsilon_m < \infty \tag{7}$$

Knowing that the ratio of $\theta^*_{max}/\theta^*_{max,0}$ is a weak function of the heat source aspect ratio (see Fig. 7), the following relationship is proposed for $\theta^*_{max}/\theta^*_{max,0}$ by curve fitting:

$$\frac{\theta^*_{max}}{\theta^*_{max,0}} = \frac{9e^{-z^*}}{(3 + z^*\sqrt{\pi\mathrm{Pe}})^2}, \quad z^* \le 1 \tag{8}$$

The proposed relationship is found to be accurate within 16% when compared against the full analytical results for $z^* \le 1$.

5 Comparison With Experimental and Numerical Data

Vick and Furey [24] computed the maximum temperature due to frictional heat generation between two sliding surfaces of square shape for the Peclet number range of $0.2 < \mathrm{Pe} < 14$. Table 3 shows the comparison between their results and those obtained from Eq. (7) with good agreement. Xu and Malkin [25] performed an experimental study to measure the temperature distribution within the workpiece of a grinding machine by using embedded thermocouples. The contact area in their work [25] is a rectangle that is elongated in the perpendicular direction of motion. The corresponding Peclet number and source aspect ratio for the experimental data are Pe=2.85 and ε_m=4.39, respectively. Other experimental conditions are listed in Table 4. Figure 8 shows that the experimental data are well predicted by Eqs. (7) and (8) with the accuracy of ±10%.

In an independent experiment, we used the proposed relationships to estimate the depth of channels engraved by a CO_2 laser system in wooden (red oak) substrates. The channel depth for a specific power and speed is estimated using Eqs. (7) and (8) by letting the maximum temperature to hold the value of autoignition temperature of red oak (i.e., the burning temperature of a material heated via radiation without any additional high-temperature heat source [20]). A value of $\alpha = 1.53 \times 10^{-7}$ $\mathrm{m}^2/\mathrm{s} \pm 5\%$ is taken as the red oak thermal diffusivity [20]

Table 3 Computed flash temperature at the surface of various sliding materials

Material	$\sqrt{A}$ (μm)	k (W/m K)	Pe	q_{mv}/q_f	$\theta_{num.}$ [24]	θ_{model}	Diff. %[a]
Al	194.4	237	1	0.57	56	56.98	−1.75
Si	28.2	148	0.2	0.51	625	649.95	−3.99
Ti	125.2	21.9	6.7	0.71	719	715.01	0.55
V	93.4	30.7	4.5	0.68	753	754.74	−0.23
Cr	90.4	93.7	1.6	0.59	296	294.38	0.55
Mn	58.2	7.8	13.4	0.77	3519	3537.44	−0.52
Fe	111.4	80	2.5	0.63	267	268.63	−0.61
Co	90.4	99.2	1.7	0.6	277	279.12	−0.77
Ni	69.6	90.7	1.5	0.59	397	400.31	−0.83
Cu	112.8	401	0.5	0.54	59	59.86	−1.46
Zn	163.8	116	2	0.61	129	129.06	−0.04
Zr	83.8	22.7	3.4	0.65	1195	1189.53	0.46
Mo	65.2	138	0.6	0.54	295	295.52	−0.18
Rh	91.4	150	0.9	0.56	189	191.14	−1.13
Pd	96.2	71.8	2	0.61	354	355.02	−0.29
Ag	112.8	429	0.3	0.53	56	57.08	−1.92
Hf	75.4	230	0.3	0.52	157	156.26	0.47
W	48.4	174	0.4	0.53	322	321.59	0.13
Pt	101	71	2	0.61	337	341.96	−1.47
Au	132.6	317	0.5	0.54	64	6.44	−0.65

[a]Diff. $\% = \theta_{num.[31]} - \theta_{model}/\theta_{num.[31]} \times 100$.

Table 4 Grinding conditions for experimental study of Xu and Malkin [25]

Parameter	Value
Wheel diameter	406 mm
Wheel width	12.5 mm
Depth of cutting	20 μm
Workpiece dimension	$44\times19\times25$ mm^3
Wheel velocity	58 m/s
Workpiece moving velocity	0.018 m/s
Temperature measurement methods	Embedded thermocouple Two color infrared detector Foil workpiece thermocouple

to compute the Peclet number. The reported auto-ignition temperature for the red oak is in the range of 420–500°C when it is irradiated by a CO_2 laser [20]. The maximum and minimum values of this range are used to compute the upper and lower bounds for the channel depth. In our calculations, the reference temperature, T_0, is assumed to hold the value of room temperature (i.e., 20°C). Figures 9 and 10 show the measured and estimated values of the channel depth as a function of the beam speed and power, respectively. Each data point in Figs. 9 and 10 is the average of at least five measured values. The error associated with the averaging method and the accuracy of the depth measurement method (±5 μm) are reported as error bars in Figs. 9 and 10. Good agreement between the estimated and measured values can be observed.

6 Summary and Conclusion

A comprehensive study on the effect of relevant geometrical parameters on the maximum temperature within a half-space due to a symmetrical moving heat source of arbitrary shape is performed in this work. The following summarizes the results of the present study.

- The heat source exact shape (e.g., corners) has a minimal effect on the maximum temperature within a half-space if the square root of source area is selected as a characteristic length throughout the analysis.
- Maximum temperature within a half-space decreases when the source speed increases. This is due to the fact that the heat source spends shorter time at each spot in higher speeds; thus, less heat is transferred to the half-space.
- For very low heat source speeds, i.e., Pe$\rightarrow$0, the effect of source orientation on the maximum temperature becomes insignificant, and the highest temperature occurs at the aspect ratio of 1 (e.g., square or circle). However, when the source speed increases, the effect of source orientation becomes significant, and the highest temperature occurs for the sources that are elongated in the direction of motion.
- The normalized maximum temperature within the half-

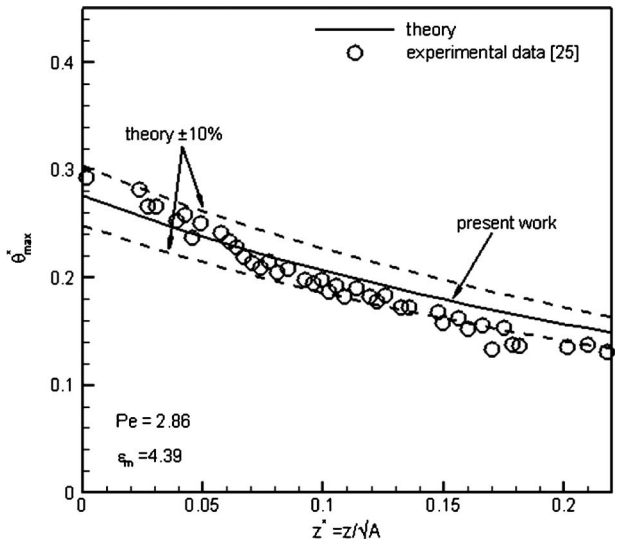

Fig. 8 Maximum dimensionless temperature in a half-space. Rectangular heat source with Pe=2.86 and aspect ratio of ε_m =4.39; experimental data from Ref. [25]; see Table 4 for the experiment parameters.

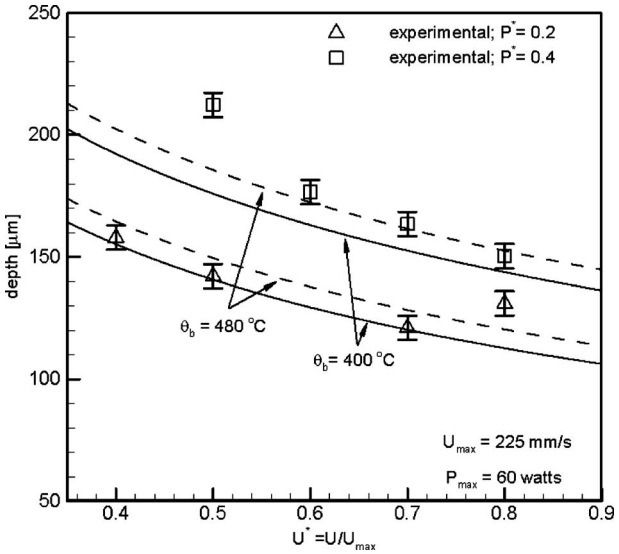

Fig. 9 Effect of laser beam speed on the depth of engraved channels using single pass ablation. Square (□) and delta (△) symbols are the present experimental measurements for percentage powers of 20% and 40%, respectively. Two limits of the reported ignition temperature are shown as the dashed line for 500°C and solid line for 420°C.

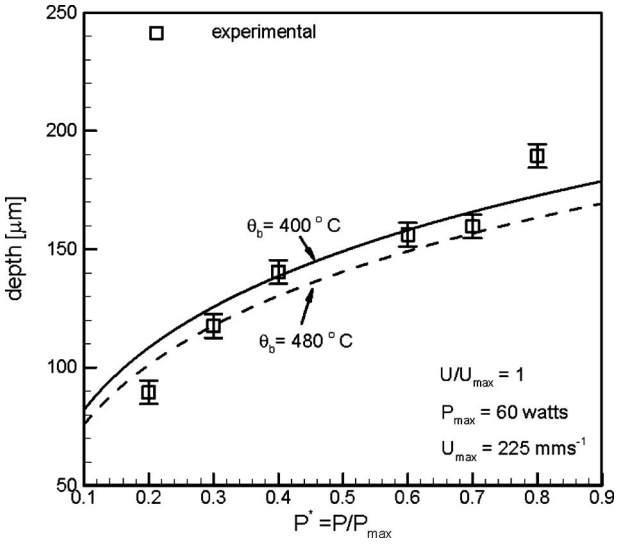

Fig. 10 Effect of laser power on the depth of engraved channels using single pass ablation at maximum beam speed. Square (□) symbols are the present experimental measurements maximum beam speed. Two limits of the reported ignition temperature are shown as the dashed line for 500°C and solid line for 420°C.

space, $\theta^*_{max}/\theta^*_{max,0}$, is found to be only a function of source speed (i.e., Peclet number). This is valid when the depth is up to the order of the length scale.

Based on the abovementioned observations, new compact relationships are proposed to predict the maximum temperature within the half-space over the entire range of Peclet numbers. In contrast to the available studies in the literature, the proposed relationship covers a wide range of symmetrical geometries and accounts for the effect of the heat source shape and orientation. The validity of the suggested relationships are examined by available experimental and numerical data for the grinding process for medium Peclet numbers, $0<\mathrm{Pe}<14$. For ultrafast heat sources ($50<\mathrm{Pe}<130$), an experimental study is performed using a commercial CO_2 laser system.

Acknowledgment

The authors gratefully acknowledge the financial support of the Natural Sciences and Engineering Research Council of Canada (NSERC), BC Innovation Council (BCIC), Canada Research Chair Program, and N. Alavi's assistance in the experimental measurements.

Nomenclature

A = heat source surface area, m^2
a = hyperellipse major axis, m
a^* = dimensionless major axis of hyperellipse
b = hyperellipse minor axis, m
b^* = dimensionless minor axis of hyperellipse
d_g = groove depth, m
d_s = laser beam size, m
F_o = Fourier number, $\alpha t/\mathcal{L}^2$
k = thermal conductivity, W/m K
n = shape parameter for hyperellipse
Pe = Peclet number, $U\mathcal{L}/2\alpha$
P^* = laser beam relative power
$\dot{q}$ = released energy per unit time per unit area, W/m^2
R^* = dimensionless distance from the origin in the moving coordinate, m
U = heat source speed, m/s
U^* = laser beam relative speed
T = temperature at any arbitrary point, K or °C
T_o = initial temperature, K or °C

Greek

α = thermal diffusivity, m^2/s
ε_m = moving source aspect ratio, b/a
ε_s = stationary source aspect ratio, b/a
$\mathcal{L}$ = characteristic length, m
θ = temperature rise $(T-T_o)$, K or °C
θ^* = dimensionless temperature rise, $\theta k/\dot{q}\mathcal{L}^2$
$\theta^*_{max,0}$ = dimensionless maximum temperature rise within a half-space due to a moving source
$\theta^*_{max,s}$ = dimensionless maximum temperature rise within a half-space due to a stationary source
$\theta^*_{max,f}$ = dimensionless maximum temperature rise of a very fast heat source
ω = absorption coefficient

References

[1] Sun, Y., Kwok, Y. C., and Nguyen, N. T., 2006, "Low-Pressure, High-Temperature Thermal Bonding of Polymeric Microfluidic Devices and Their Applications for Electrophoretic Separation," J. Micromech. Microeng., **16**, pp. 1681–1688.
[2] Kricka, L. J., Fortina, P., Panaro, N. J., Wilding, P., Alonso-Amigo, G., and Becker, H., 2002, "Fabrication of Plastic Microchips by Hot Embossing," Lab Chip, **2**(1), pp. 1–4.
[3] Halling, J., 1975, *Principles of Tribology*, Macmillan, London.
[4] Williams, J. A., 2005, *Engineering Tribology*, Cambridge University Press, Cambridge, UK.
[5] Winer, W. O., and Cheng, H. S., 1980, "Film Thickness, Contact Stress and Surface Temperatures," *Wear Control Handbook*, ASME, New York, pp. 81–141.
[6] Tian, X., and Kennedy, F. E., Jr., 1994, "Maximum and Average Flash Temperatures in Sliding Contacts," ASME J. Tribol., **116**, pp. 167–174.
[7] Hou, Z. B., and Komanduri, R., 2000, "General Solutions for Stationary/Moving Plane Heat Source Problems in Manufacturing and Tribology," Int. J. Heat Mass Transfer, **43**(10), pp. 1679–1698.
[8] Laraqi, N., Baïri, A., and Segui, L., 2004, "Temperature and Thermal Resistance in Frictional Devices," Appl. Therm. Eng., **24**(17–18), pp. 2567–2581.
[9] Carslaw, H. S., and Jaeger, J. C., 1959, *Conduction of Heat in Solids*, Oxford University Press, New York.
[10] Muzychka, Y. S., and Yovanovich, M. M., 2001, "Thermal Resistance Models for Non-Circular Moving Heat Sources on a Half Space," ASME J. Heat Transfer, **123**(4), pp. 624–632.
[11] Rosenthal, D., 1946, "The Theory of Moving Sources of Heat and Its Application to Metal Treatments," Trans. ASME, **68**(11), pp. 849–866.
[12] Weichert, R., and Schonert, K., 1978, "Temperature Distribution Produced by a Moving Heat Source," Q. J. Mech. Appl. Math., **31**(3), pp. 363–379.
[13] Terauchi, Y., Nadano, H., and Kohno, M., 1985, "On the Temperature Rise Caused by Moving Heat Sources. II: Calculation of Temperature Considering Heat Radiation From Surface," Bull. JSME, **28**(245), pp. 2789–2795.
[14] Yovanovich, M. M., 1997, "Transient spreading resistance of arbitrary isoflux contact areas-development of a universal time function," presented at the 32nd AIAA Thermophysics Conference, Atlanta, GA.
[15] Yovanovich, M. M., Negus, K. J., and Thompson, J. C., 1984, "Transient Temperature Rise of Arbitrary Contacts With Uniform Flux by Surface Element Methods," presented at the 22nd AIAA Aerospace Sciences Meeting, Reno, NV, Jan. 9–12.
[16] www.maplesoft.com
[17] Simms, D. L., 1960, "Ignition of Cellulosic Materials by Radiation," Combust. Flame, **4**, pp. 293–300.
[18] Koohyar, A. N., 1967, *Ignition of Wood by Flame Radiation*, University of Oklahoma, Norman, OK.
[19] Kashiwagi, T., 1979, "Experimental Observation of Radiative Ignition Mechanisms," Combust. Flame, **34**, pp. 231–244.
[20] Kashiwagi, T., 1979, "Effects of Attenuation of Radiation on Surface Temperature for Radiative Ignition," Combust. Sci. Technol., **20**(5), pp. 225–234.
[21] Wesson, H. R., 1970, *The Piloted Ignition of Wood by Radiant Heat*, University of Oklahoma, Norman, OK.
[22] Taylor, J. R., 1997, *An Introduction to Error Analysis: The Study of Uncertainties in Physical Measurements*, University Science Books, Herndon, VA.
[23] Jaeger, J. C., 1942, "Moving Sources of Heat and the Temperature at Sliding Contacts," J. Proc. R. Soc. N. S. W., **76**, pp. 203–224.
[24] Vick, B., and Furey, M. J., 2003, "An Investigation Into the Influence of Frictionally Generated Surface Temperatures on Thermionic Emission," Wear, **254**(11), pp. 1155–1161.
[25] Xu, X., and Malkin, S., 2001, "Comparison of Methods to Measure Grinding Temperatures," ASME J. Manuf. Sci. Eng., **123**, pp. 191–195.
[26] Takazawa, K., 1966, "Effects of Grinding Variables on Surface Structure of Hardened Steel," Bull. Jap. Soc. Grind Eng., **6**, pp. 14–19.
[27] Paek, U.-C., and Gagliano, F., 1972, "Thermal Analysis of Laser Drilling Processes," IEEE J. Quantum Electron., **8**(2), pp. 112–119.
[28] Eagar, T. W., and Tsai, N. S., 1983, "Temperature Fields Produced by Traveling Distributed Heat Sources," Weld. J. (Miami, FL, U.S.), **62**(12), pp. 346–355.
[29] Zhang, H. J., 1990, "Non-Quasi-Steady Analysis of Heat Conduction From a Moving Heat Source," ASME Trans. J. Heat Transfer, **112**, pp. 777–779.
[30] Manca, O., Morrone, B., and Naso, V., 1995, "Quasi-Steady-State Three-Dimensional Temperature Distribution Induced by a Moving Circular Gaussian Heat Source in a Finite Depth Solid," Int. J. Heat Mass Transfer, **38**(7), pp. 1305–1315.
[31] Yevtushenko, A. A., Ivanyk, E. G., and Ukhanska, O. M., 1997, "Transient Temperature of Local Moving Areas of Sliding Contact," Tribol. Int., **30**(3), pp. 209–214.
[32] Zeng, Z., Brown, J. M. B., and Vardy, A. E., 1997, "On Moving Heat Sources," Heat Mass Transfer, **33**(1–2), pp. 41–49.
[33] Zubair, S. M., and Chaudhry, M. A., 1998, "A Unified Approach to Closed-Form Solutions of Moving Heat-Source Problems," Heat Mass Transfer, **33**(5–6), pp. 415–424.
[34] Zubair, S. M., and Chaudhry, M. A., 1996, "Temperature Solutions Due to Time-Dependent Moving-Line-Heat Sources," Heat Mass Transfer, **31**(3), pp. 185–189.
[35] Kato, T., and Fujii, H., 1997, "Temperature Measurement of Workpiece in Surface Grinding by PVD Film Method," ASME J. Manuf. Sci. Eng., **119**, pp. 689–694.
[36] Kaebernick, H., Bicleanu, D., and Brandt, M., 1999, "Theoretical and Experimental Investigation of Pulsed Laser Cutting," CIRP Ann., **48**(1), pp. 163–166.
[37] Neder, Z., Varadi, K., Man, L., and Friedrich, K., 1999, "Numerical and Finite Element Contact Temperature Analysis of Steel-Bronze Real Surfaces in Dry Sliding Contact," Tribol. Trans., **42**(3), pp. 453–462.
[38] Baïri, A., 2003, "Analytical Model for Thermal Resistance Due to Multiple Moving Circular Contacts on a Coated Body," C. R. Mec., **331**(8), pp. 557–562.

[39] Li, J. F., Li, L., and Stott, F. H., 2004, "Comparison of Volumetric and Surface Heating Sources in the Modeling of Laser Melting of Ceramic Materials," Int. J. Heat Mass Transfer, **47**(6–7), pp. 1159–1174.
[40] Kuo, W. L., and Lin, J. F., 2006, "General Temperature Rise Solution for a Moving Plane Heat Source Problem in Surface Grinding," Int. J. Adv. Manuf. Technol., **31**(3–4), pp. 268–277.
[41] Bianco, N., Manca, O., Nardini, S., and Tamburrino, S., 2006, "Transient Heat Conduction in Solids Irradiated by a Moving Heat Source," presented at the Proceedings of COMSOL Users Conference, Milan.
[42] Wen, J., and Khonsari, M. M., 2007, "Analytical Formulation for the Temperature Profile by Duhamel's Theorem in Bodies Subjected to an Oscillatory Heat Source," ASME J. Heat Transfer, **129**, pp. 236–240.
[43] Levin, P., 2008, "A General Solution of 3-D Quasi-Steady-State Problem of a Moving Heat Source on a Semi-Infinite Solid," Mech. Res. Commun., **35**(3), pp. 151–157.
[44] Laraqi, N., Alilat, N., de Maria, J. M., and Bāīri, A., 2009, "Temperature and Division of Heat in a Pin-on-Disc Frictional Device—Exact Analytical Solution," Wear, **266**(7–8), pp. 765–770.
[45] Xu, H., Chen, W. W., Zhou, K., Huang, Y., and Wang, Q. J., 2010, "Temperature Field Computation for a Rotating Cylindrical Workpiece Under Laser Quenching," Int. J. Adv. Manuf. Technol., **47**(5–8), pp. 679–686.